Physical point simulation in 2 + 1 flavor lattice QCD

S. Aoki,[1,2] K.-I. Ishikawa,[4] N. Ishizuka,[1,3] T. Izubuchi,[2,5] D. Kadoh,[3,*] K. Kanaya,[1] Y. Kuramashi,[1,3] Y. Namekawa,[3]
M. Okawa,[4] Y. Taniguchi,[1,3] A. Ukawa,[1,3] N. Ukita,[3] T. Yamazaki,[3] and T. Yoshié[1,3]

(PACS-CS Collaboration)

[1]*Graduate School of Pure and Applied Sciences, University of Tsukuba, Tsukuba, Ibaraki 305-8571, Japan*
[2]*Riken BNL Research Center, Brookhaven National Laboratory, Upton, New York 11973, USA*
[3]*Center for Computational Sciences, University of Tsukuba, Tsukuba, Ibaraki 305-8577, Japan*
[4]*Graduate School of Science, Hiroshima University, Higashi-Hiroshima, Hiroshima 739-8526, Japan*
[5]*Institute for Theoretical Physics, Kanazawa University, Kanazawa, Ishikawa 920-1192, Japan*
(Received 13 November 2009; revised manuscript received 7 February 2010; published 14 April 2010)

We present the results of the physical point simulation in 2 + 1 flavor lattice QCD with the nonperturbatively $O(a)$-improved Wilson quark action and the Iwasaki gauge action at $\beta = 1.9$ on a $32^3 \times 64$ lattice. The physical quark masses together with the lattice spacing is determined with m_π, m_K and m_Ω as physical inputs. There are two key algorithmic ingredients to make possible the direct simulation at the physical point: One is the mass-preconditioned domain-decomposed HMC algorithm to reduce the computational cost. The other is the reweighting technique to adjust the hopping parameters exactly to the physical point. The physics results include the hadron spectrum, the quark masses and the pseudoscalar meson decay constants. The renormalization factors are nonperturbatively evaluated with the Schrödinger functional method. The results are compared with the previous ones obtained by the chiral extrapolation method.

I. INTRODUCTION

The physical point simulation is one of the essential ingredients in the first principle calculation of lattice QCD. However, it is still a tough challenge because of the rapid growth of the computational cost with the up-down (ud) quark mass reduced toward its physical value. At present, simulation points are typically restricted to $m_\pi \gtrsim 250$ MeV. The most popular strategy to obtain the results at the physical point is chiral extrapolation with the use of chiral perturbation theory (ChPT) as a guiding principle. This strategy, however, has several problems: (i) It is numerically difficult to precisely trace the logarithmic quark mass dependence of the physical quantities predicted by ChPT. (ii) It may not be always possible to resort to ChPT as a good guiding principle for chiral extrapolation. (iii) The kinematics changes as the quark mass increases. A typical example is the $\rho \rightarrow \pi\pi$ decay which is not allowed for the increased ud quark mass away from the physical value. (iv) Our final destination is to incorporate the different up and down quark masses. The isospin breaking effects are so tiny that reliable evaluation would be difficult by the chiral extrapolation method.

In this article we present the results of the physical point simulation which has been pursued as the PACS-CS project

based on the PACS-CS (parallel array computer system for computational sciences) computer with a peak speed of 14.3 Tflops developed at University of Tsukuba [1–3]. The simulation is carried out with the nonperturbatively $O(a)$-improved Wilson quark action [4] and the Iwasaki gauge action [5] on a $(3 \text{ fm})^3$ box at the lattice spacing of $a = 0.089\,95(40)$ fm. There are two types of problems in the physical point simulation. First, we need to reduce the computational cost which rapidly increases as the ud quark mass decreases. This difficulty is overcome thanks to the domain-decomposed HMC (DDHMC) algorithm [6] with the mass preconditioning [7,8]. In Refs. [9,10] this algorithm was successfully applied to investigate the chiral behaviors of the pseudoscalar meson sector and the hadron masses including both the mesons and the baryons, where the pion mass covers from 156 MeV to 702 MeV. The second problem is fine-tuning of the quark masses to the physical point after we reach around the physical point. This task is accomplished with the reweighting technique which allows us to cover a small variation of simulation parameters in a single Monte Carlo run [11]. We explain the details of the method and present the physics results on the physical point without interpolation or extrapolation.

This paper is organized as follows. In Sec. II we present the simulation details including the parameters and the algorithm. Section III is devoted to describe the reweighting method. We present the physics results on the physical point in Sec. IV. Our conclusions are summarized in Sec. V.

*Present address: Theoretical Physics Laboratory, RIKEN, Wako 2-1, Saitama 351-0198, Japan.

II. SIMULATION DETAILS

A. Actions

We employ the Iwasaki gauge action [5] and the nonperturbatively $O(a)$-improved Wilson quark action as in the previous works [9,12]. The former is composed of a plaquette and a 1×2 rectangle loop:

$$S_{\text{g}} = \frac{1}{g^2}\left\{ c_0 \sum_{\text{plaquette}} \text{tr}U_{\text{pl}} + c_1 \sum_{\text{rectangle}} \text{tr}U_{\text{rtg}} \right\} \quad (1)$$

with $c_1 = -0.331$ and $c_0 = 1 - 8c_1 = 3.648$. The latter is expressed as

$$S_{\text{quark}} = \sum_{q=\text{u,d,s}}\left[\sum_n \bar{q}_n q_n - \kappa_q c_{\text{SW}} \sum_n \sum_{\mu,\nu} \frac{i}{2} \bar{q}_n \sigma_{\mu\nu} F_{\mu\nu}(n) q_n \right.$$
$$- \kappa_q \sum_n \sum_\mu \{\bar{q}_n (1 - \gamma_\mu) U_{n,\mu} q_{n+\hat{\mu}}$$
$$\left. + \bar{q}_n (1 + \gamma_\mu) U^\dagger_{n-\hat{\mu},\mu} q_{n-\hat{\mu}} \} \right], \quad (2)$$

where we consider the case of a degenerate up and down quark mass $\kappa_{\text{u}} = \kappa_{\text{d}}$. The Euclidean gamma matrices are defined in terms of the Minkowski matrices in the Bjorken-Drell convention: $\gamma_j = -i\gamma^j_{\text{BD}}$ ($j = 1, 2, 3$), $\gamma_4 = \gamma^0_{\text{BD}}$, $\gamma_5 = \gamma^5_{\text{BD}}$, and $\sigma_{\mu\nu} = \frac{1}{2}[\gamma_\mu, \gamma_\nu]$. The field strength $F_{\mu\nu}$ in the clover term is given by

$$F_{\mu\nu}(n) = \frac{1}{4} \sum_{i=1}^4 \frac{1}{2i}(U_i(n) - U^\dagger_i(n)), \quad (3)$$

$$U_1(n) = U_{n,\mu} U_{n+\hat{\mu},\nu} U^\dagger_{n+\hat{\nu},\mu} U^\dagger_{n,\nu}, \quad (4)$$

$$U_2(n) = U_{n,\nu} U^\dagger_{n-\hat{\mu}+\hat{\nu},\mu} U^\dagger_{n-\hat{\mu},\nu} U_{n-\hat{\mu},\mu}, \quad (5)$$

$$U_3(n) = U^\dagger_{n-\hat{\mu},\mu} U^\dagger_{n-\hat{\mu}-\hat{\nu},\nu} U_{n-\hat{\mu}-\hat{\nu},\mu} U_{n-\hat{\nu},\nu}, \quad (6)$$

$$U_4(n) = U^\dagger_{n-\hat{\nu},\nu} U_{n-\hat{\nu},\mu} U_{n+\hat{\mu}-\hat{\nu},\nu} U^\dagger_{n,\mu}. \quad (7)$$

The improvement coefficient c_{SW} for $O(a)$ improvement was determined nonperturbatively in Ref. [4].

B. Simulation parameters

Simulations are performed employing the same parameters as in the previous work [9]: a $32^3 \times 64$ lattice at $\beta = 1.90$ with $c_{\text{SW}} = 1.715$ [4]. We choose $(\kappa_{\text{ud}}, \kappa_{\text{s}}) = (0.137\,785\,00, 0.136\,600\,00)$ for a degenerate pair of up and down quarks and a strange quark. This combination of the hopping parameters was supposed to be the physical point based on the analysis of the previous results [9]. The lattice spacing is determined as $a = 0.08995(40)$ fm from the m_π, m_K, m_Ω results on the physical point after the reweighting procedure. Table I summarizes the run parameters. After thermalization we calculate hadronic observables solving quark propagators at every 20 trajectories

TABLE I. Simulation parameters. MD time is the number of trajectories multiplied by the trajectory length τ.

κ_{ud}	0.137 785
κ_{s}	0.136 600
#run	5
τ	0.25
block size	8^4
$(N_0, N_1, N_2, N_3, N_4)$	(4, 4, 2, 4, 4)
ρ_1	0.9995
ρ_2	0.9900
N_{poly}	220
Replay	off
MD time	2000
$\langle P \rangle$	0.571 082(9)
$\langle e^{-dH} \rangle$	0.9916(81)
$P_{\text{acc}}(\text{HMC})$	0.8109(45)
$P_{\text{acc}}(\text{GMP})$	0.9519(27)

(5 MD time units), while we measure the plaquette expectation value at every trajectory. The reweighting factors for the up-down and the strange quarks are evaluated at every 100 trajectories (25 MD time units). The choice of sparse measurements is due to the demanding computational cost of the reweighting factors. The hadronic observables measured at every 20 and 100 trajectories show consistency within error bars. For the pion mass we find that the former has larger magnitude of error: 0.0719(37) and 0.0693(27). This could be due to wavy behavior of pion propagators on a couple of configurations caused by the statistical fluctuation.

C. Algorithm

Our base algorithm for the degenerate up-down quarks is the DDHMC algorithm [6] which makes a geometric separation of the up-down quark determinant into the UV and the IR parts with the domain-decomposition of the full lattice into small blocks. This UV/IR separation naturally introduces the multiple time integration scheme [13] in the molecular dynamics (MD) steps. We employ the nested simple leapfrog with QPQ ordering for the multiple time step MD integrator. According to the relative magnitude of the force terms coming from the gauge part and the UV and the IR parts of the up-down quarks we choose the associated step sizes such that

$$\delta\tau_{\text{g}} \|F_{\text{g}}\| \approx \delta\tau_{\text{UV}} \|F_{\text{UV}}\| \approx \delta\tau_{\text{IR}} \|F_{\text{IR}}\|, \quad (8)$$

where $\delta\tau_{\text{g}} = \tau/N_0 N_1 N_2$, $\delta\tau_{\text{UV}} = \tau/N_1 N_2$, $\delta\tau_{\text{IR}} = \tau/N_2$ with τ the trajectory length and (N_0, N_1, N_2) a set of integers to control the step sizes.

In the previous work we used the mass-preconditioned DDHMC (MPDDHMC) algorithm for the run at $(\kappa_{\text{ud}}, \kappa_{\text{s}}) = (0.137\,810\,00, 0.136\,400\,00)$ which gives the lightest up-down quark mass [9]. A preconditioner controlled by an additional hopping parameter $\kappa'_{\text{ud}} = \rho\kappa_{\text{ud}}$ is

incorporated to tame the fluctuation of the IR force F_{IR} in the original DDHMC algorithm by dividing it into $\tilde{F}_{IR}$ and F'_{IR}. The former is derived from the preconditioned action and the latter from the preconditioner. In this work we employ twofold-mass-preconditioned DDHMC (MP^{2}DDHMC) algorithm which split F_{IR} into $\tilde{F}_{IR}$, F'_{IR} and F''_{IR}. This decomposition is controlled by two additional hopping parameters $\kappa'_{ud} = \rho_1 \kappa$ and $\kappa''_{ud} = \rho_1 \rho_2 \kappa$. $\tilde{F}_{IR}$ is derived from the action preconditioned with κ'_{ud}. The ratio of two preconditioners with κ'_{ud} and κ''_{ud} gives F'_{IR}. F''_{IR} is from the heaviest preconditioners with κ''_{ud}. We find the following relative magnitude for the force terms:

$$\|F_g\|:\|F_{UV}\|:\|F''_{IR}\|:\|F'_{IR}\|:\|\tilde{F}_{IR}\| \approx 16:4:1:1/7:1/60 \quad (9)$$

with $\rho_1 = 0.9995$ and $\rho_2 = 0.9900$. We choose $(N_0, N_1, N_2, N_3, N_4) = (4, 4, 2, 4, 4)$ for the associated step sizes: $\delta\tau_g = \tau/N_0 N_1 N_2 N_3 N_4$, $\delta\tau_{UV} = \tau/N_1 N_2 N_3 N_4$, $\delta\tau''_{IR} = \tau/N_2 N_3 N_4$, $\delta\tau'_{IR} = \tau/N_3 N_4$, $\delta\tilde{\tau}_{IR} = \tau/N_4$. This choice results in rather high acceptance rate found in Table I. The replay trick [6,14] is not incorporated.

For the inversion of the Wilson-Dirac operator during the MD steps we implement the same algorithmic techniques as for the run at $(\kappa_{ud}, \kappa_s) = (0.137\,810\,00,$ $0.136\,400\,00)$ in the previous work [9]. There are three important points to be noted. First, the initial solution vector is provided by the chronological guess with the last 16 solutions [15]. We demand a stringent stopping condition $|Dx - b|/|b| < 10^{-14}$ to assure the reversibility. Second, the inversion algorithm is a nested BiCGStab solver consisting of an inner and an outer solvers. The former plays the role of a preconditioner whose calculation is accelerated by single precision arithmetic with an automatic tolerance control ranging from 10^{-3} to 10^{-6}. The

latter is implemented with double precision imposing a stringent tolerance of 10^{-14}. Third, the deflation technique is incorporated in a nested BiCGStab algorithm: Once the inner solver becomes stagnant during the inversion of the Wilson-Dirac operator, the solver algorithm is automatically replaced by the GCRO-DR (generalized conjugate residual with implicit inner orthogonalization and deflated restarting) algorithm [16]. This saves us from the difficulties due to possible small eigenvalues allowed in the Wilson-type quark action. We refer to Appendix B in Ref. [9] for more details of the inversion algorithm.

The strange quark is simulated with the UV-filtered PHMC (UVPHMC) algorithm [17–20] where the action is UV-filtered [21] after the even-odd site preconditioning without domain-decomposition. We set the step size as $\delta\tau_s = \delta\tau''_{IR}$ according to our observation $\|F_s\| \approx \|F_{IR}\|$. This algorithm is made exact by correcting the polynomial approximation with the global metropolis test [22] at the end of each trajectory. In Table I we find that the choice of $N_{poly} = 220$ yields 95% acceptance rate.

III. REWEIGHTING METHOD

A. Formalism

Let us consider evaluating $\langle \mathcal{O}[U](\kappa^*_{ud}, \kappa^*_s)\rangle_{(\kappa^*_{ud}, \kappa^*_s)}$, which is the expectation value of a physical observable $\mathcal{O}$ at the target hopping parameters $(\kappa^*_{ud}, \kappa^*_s)$, using the configuration samples generated at the original hopping parameters (κ_{ud}, κ_s). We assume that $\rho_{ud} \equiv \kappa_{ud}/\kappa^*_{ud} \simeq 1$ and $\rho_s \equiv \kappa_s/\kappa^*_s \simeq 1$. With this assumption, the expectation value is rewritten as follows using the single histogram reweighting method [11]:

$$
\begin{aligned}
\langle \mathcal{O}[U](\kappa^*_{ud}, \kappa^*_s)\rangle_{(\kappa^*_{ud}, \kappa^*_s)} &= \frac{\int \mathcal{D}U \mathcal{O}[U](\kappa^*_{ud}, \kappa^*_s) |\det[D_{\kappa^*_{ud}}[U]]|^2 \det[D_{\kappa^*_s}[U]]e^{-S_g[U]}}{\int \mathcal{D}U |\det[D_{\kappa^*_{ud}}[U]]|^2 \det[D_{\kappa^*_s}[U]]e^{-S_g[U]}} \\
&= \frac{\int \mathcal{D}U \mathcal{O}[U](\kappa^*_{ud}, \kappa^*_s) |\det[\frac{D_{\kappa^*_{ud}}[U]}{D_{\kappa_{ud}}[U]}]|^2 \det[\frac{D_{\kappa^*_s}[U]}{D_{\kappa_s}[U]}] |\det[D_{\kappa_{ud}}[U]]|^2 \det[D_{\kappa_s}[U]]e^{-S_g[U]}}{\int \mathcal{D}U |\det[\frac{D_{\kappa^*_{ud}}[U]}{D_{\kappa_{ud}}[U]}]|^2 \det[\frac{D_{\kappa^*_s}[U]}{D_{\kappa_s}[U]}] |\det[D_{\kappa_{ud}}[U]]|^2 \det[D_{\kappa_s}[U]]e^{-S_g[U]}} \\
&= \frac{\langle \mathcal{O}[U](\kappa^*_{ud}, \kappa^*_s) R_{ud}[U] R_s[U]\rangle_{(\kappa_{ud}, \kappa_s)}}{\langle R_{ud}[U] R_s[U]\rangle_{(\kappa_{ud}, \kappa_s)}},
\end{aligned}
\quad (10)
$$

where the reweighting factors are defined as

$$R_{ud}[U] = \left|\det\left[\frac{D_{\kappa^*_{ud}}[U]}{D_{\kappa_{ud}}[U]}\right]\right|^2, \quad (11)$$

$$R_s[U] = \det\left[\frac{D_{\kappa^*_s}[U]}{D_{\kappa_s}[U]}\right] \quad (12)$$

and

$$D_{\kappa_q}[U] = 1 + \kappa_q(T + M) (q = ud, s) \quad (13)$$

with T the local clover term including the nonperturbative c_{SW} and M the hopping matrix. The above expression (10) demands us to evaluate the reweighting factors $R_{ud}[U]$ and $R_s[U]$ on each configuration. For later convenience we define
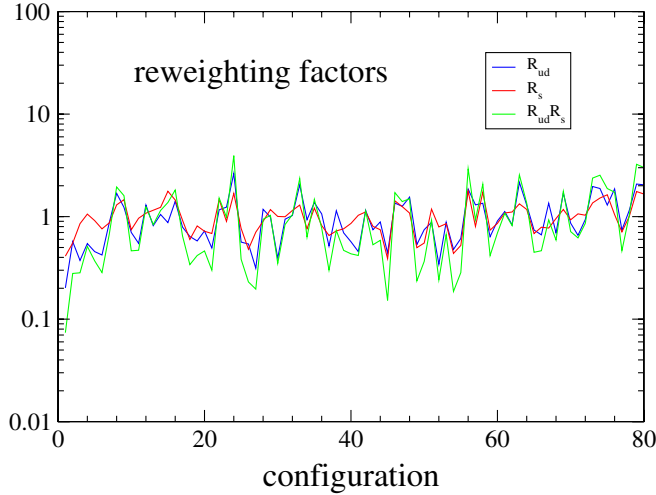
$$W[U](\rho_q) \equiv \frac{D_{\kappa_q^*}[U]}{D_{\kappa_q}[U]} \qquad (14)$$

with $\rho_q = \kappa_q/\kappa_q^*$.

B. Evaluation of reweighting factors

The reweighting factor $R_{ud}[U]$ can be evaluated with a stochastic method. Introducing a complex bosonic field η, whose spin and color indices are suppressed here, the determinant of W is expressed as

$$
\begin{aligned}
R_{ud}[U] &= |\det[W[U](\rho_{ud})]|^2 \\
&= \frac{\int \mathcal{D}\eta^\dagger \mathcal{D}\eta e^{-|W^{-1}[U](\rho_{ud})\eta|^2}}{\int \mathcal{D}\eta^\dagger \mathcal{D}\eta e^{-|\eta|^2}} \\
&= \frac{\int \mathcal{D}\eta^\dagger \mathcal{D}\eta e^{-|W^{-1}[U](\rho_{ud})\eta|^2+|\eta|^2-|\eta|^2}}{\int \mathcal{D}\eta^\dagger \mathcal{D}\eta e^{-|\eta|^2}} \\
&= \langle e^{-|W^{-1}[U](\rho_{ud})\eta|^2+|\eta|^2} \rangle_\eta, \qquad (15)
\end{aligned}
$$

where $\langle \cdots \rangle_\eta$ means the expectation value with respect to η. Given a set of $\eta^{(i)}$ ($i = 1, \ldots, N_\eta$) which are random noises generated according to the Gaussian distribution, the reweighting factor is evaluated as

$$R_{ud}[U] = \lim_{N_\eta \to \infty} \frac{1}{N_\eta} \sum_{i=1}^{N_\eta} e^{-|W^{-1}[U](\rho_{ud})\eta|^2+|\eta|^2}. \qquad (16)$$

The ratio W^{-1} is further simplified as follows:

$$W^{-1}[U](\rho_{ud}) = \frac{D_{\kappa_{ud}}[U]}{D_{\kappa_{ud}^*}[U]} = \rho_{ud} + (1 - \rho_{ud})D_{\kappa_{ud}^*}^{-1}[U] \qquad (17)$$

with the use of $D_{\kappa_{ud}}[U] = \rho_{ud}D_{\kappa_{ud}^*}[U] + (1 - \rho_{ud})$. We just need $D_{\kappa_{ud}^*}^{-1}$ to calculate W^{-1}.

For the strange quark we assume that $\det[W[U](\rho_s)]$ is positive. The corresponding reweighting factor is evaluated as

$$
\begin{aligned}
R_s[U] &= \det[W[U](\rho_s)] \\
&= \frac{\int \mathcal{D}\eta^\dagger \mathcal{D}\eta e^{-|W^{-1/2}[U](\rho_s)\eta|^2}}{\int \mathcal{D}\eta^\dagger \mathcal{D}\eta e^{-|\eta|^2}} \\
&= \frac{\int \mathcal{D}\eta^\dagger \mathcal{D}\eta e^{-|W^{-1/2}[U](\rho_s)\eta|^2+|\eta|^2-|\eta|^2}}{\int \mathcal{D}\eta^\dagger \mathcal{D}\eta e^{-|\eta|^2}} \\
&= \langle e^{-|W^{-1/2}[U](\rho_s)\eta|^2+|\eta|^2} \rangle_\eta. \qquad (18)
\end{aligned}
$$

With the assumption of $\rho_s \simeq 1$ we expect that $W[U](\rho_s)$ is so close to the identity matrix that its eigenvalues are enclosed by a unit circle centered at $(1, 0)$ in the complex plane. In this case we can evaluate $W^{-1/2}[U](\rho_s)\eta$ by the Taylor expansion around identity.

To evaluate the matrix square root $W^{-1/2}[U](\rho_s)$ we first parametrize $W^{-1}[U](\rho_s)$ as

$$
\begin{aligned}
W^{-1}[U](\rho_s) &= \frac{D_{\kappa_s}[U]}{D_{\kappa_s^*}[U]} = \rho_s + (1 - \rho_s)D_{\kappa_s^*}^{-1}[U] \\
&= 1 - (1 - \rho_s)(1 - D_{\kappa_s^*}^{-1}[U]) \\
&= 1 - X[U](\rho_s) \qquad (19)
\end{aligned}
$$

where $|1 - \rho_s| \ll 1$ and $\|X[U](\rho_s)\| < 1$. We employ the recursive expression for the Taylor expansion of $W^{-1/2}[U](\rho_s)\eta$ [19]:

$$
\begin{aligned}
W^{-1/2}\eta &= \sum_{j=0}^{N} c_j X^j \eta \\
&= c_0 \Bigg[\eta + \frac{c_1}{c_0} X \Bigg[\eta + \frac{c_2}{c_1} X \\
&\quad \times \Bigg[\eta + \frac{c_3}{c_2} X \Bigg[\cdots \Bigg[\eta + \frac{c_{N-1}}{c_{N-2}} X \\
&\quad \times \Bigg[\eta + \frac{c_N}{c_{N-1}} X \eta \Bigg] \Bigg] \Bigg] \Bigg] \Bigg] \Bigg], \qquad (20)
\end{aligned}
$$

where the argument $[U](\rho_s)$ for the matrices is suppressed. The coefficients are given by

$$\frac{c_j}{c_{j-1}} = 1 - \frac{3}{2j} \qquad (21)$$

with $c_0 = 1$. The advantage of the recursive procedure is to reduce the round-off errors in the summation from the lower-order to the higher-order contributions in the Taylor expansion. The truncation error and the order of the Taylor expansion N are monitored and controlled during the simulation by explicitly evaluating the residual $r = \|(W^{-1/2}W^{-1/2} - W^{-1})\eta\|//\|\eta\|$. We enforce the condition $r < 10^{-14}$ for N.

To reduce the fluctuations in the stochastic evaluation of $R_{ud}[U]$ and $R_s[U]$ we employ the determinant breakup technique [23,24]. The interval between κ_q and κ_q^* is divided into N_B subintervals: $\{\kappa_q, \kappa_q + \Delta_q, \ldots, \kappa_q + (N_B - 1)\Delta_q, \kappa_q^*\}$ with $\Delta_q = (\kappa_q^* - \kappa_q)/N_B$. Thus the determinant of $W[U](\rho_q)$ is broken up as

$$
\begin{aligned}
\det[W[U](\rho_q)] &= \det\Bigg[W[U]\Big(\frac{\kappa_q}{\kappa_q + \Delta_q}\Big) \Bigg] \\
&\quad \cdot \det\Bigg[W[U]\Big(\frac{\kappa_q + \Delta_q}{\kappa_q + 2\Delta_q}\Big) \Bigg] \\
&\quad \cdots \det\Bigg[W[U]\Big(\frac{\kappa_q + (N_B - 1)\Delta_q}{\kappa_q^*}\Big) \Bigg],
\end{aligned}
$$
$$(22)$$

where each determinant in the right-hand side is evaluated with an independent noise set of η. For strange quark reweighting, W^{-1} are simply replaced by $W^{-1/2}$ in Eq. (22).

FIG. 1 (color online). Configuration dependence of reweighting factors from $(\kappa_{\text{ud}}, \kappa_{\text{s}}) = (0.137\,785\,00, 0.136\,600\,00)$ to $(\kappa_{\text{ud}}^*, \kappa_{\text{s}}^*) = (0.137\,796\,25, 0.136\,633\,75)$.

FIG. 2 (color online). Reweighting factors from $(\kappa_{\text{ud}}, \kappa_{\text{s}}) = (0.137\,785\,00, 0.136\,600\,00)$ to $(\kappa_{\text{ud}}^*, \kappa_{\text{s}}^*) = (0.137\,796\,25, 0.136\,633\,75)$ as a function of plaquette value.

C. Parameters and results for reweighting factors

Our choice of the target hopping parameters are $(\kappa_{\text{ud}}^*, \kappa_{\text{s}}^*) = (0.137\,796\,25, 0.136\,633\,75)$. The subintervals for the determinant breakup are $\Delta_{\text{ud}} = (0.137\,796\,25 - 0.137\,785\,00)/N_B$ with $N_B = 3$ for the ud quark and $\Delta_{\text{s}} = (0.136\,633\,75 - 0.136\,600\,00)/N_B$ with $N_B = 3$ for the s quark. Each piece of the divided determinant is evaluated stochastically employing 10 sets of η at every 100 trajectories (25 MD time units). The order of Taylor expansion N was mostly 5 for each of the strange quark reweighting break up.

Figure 1 shows configuration dependence of the reweighting factors from $(\kappa_{\text{ud}}, \kappa_{\text{s}}) = (0.137\,785\,00, 0.136\,600\,00)$ to $(\kappa_{\text{ud}}^*, \kappa_{\text{s}}^*) = (0.137\,796\,25, 0.136\,633\,75)$ which are normalized as $\langle R_{\text{ud,s}} \rangle = 1$ and $\langle R_{\text{ud}} R_{\text{s}} \rangle = 1$. The fluctuations of R_{ud} and R_{s} are within a factor of 10. Their product has slightly amplified fluctuations. In Fig. 2 we plot the reweighting factors as a function of the plaquette value on each configuration. An important observation is a clear correlation between the reweighting factors and the plaquette value: The former increases as the latter becomes larger. Thanks to this correlation the distribution of the plaquette value at $(\kappa_{\text{ud}}^*, \kappa_{\text{s}}^*) = (0.137\,796\,25, 0.136\,633\,75)$ is moved in the positive direction. This is the expected behavior, because the target hopping parameters are larger than the original ones. The situation is quantitatively illustrated in Fig. 3, where the reweighted plaquette values with R_{ud} and R_{s} are individually plotted as a function of the number of noise. The results look converged once the number of noise goes beyond four.

Since the formula of Eq. (10) is the identity, the reweighting procedure is always assured if we have infinite statistics. In case of finite statistics in practical simulations, however, we should be concerned with the possible situation that the original and the target points are far away
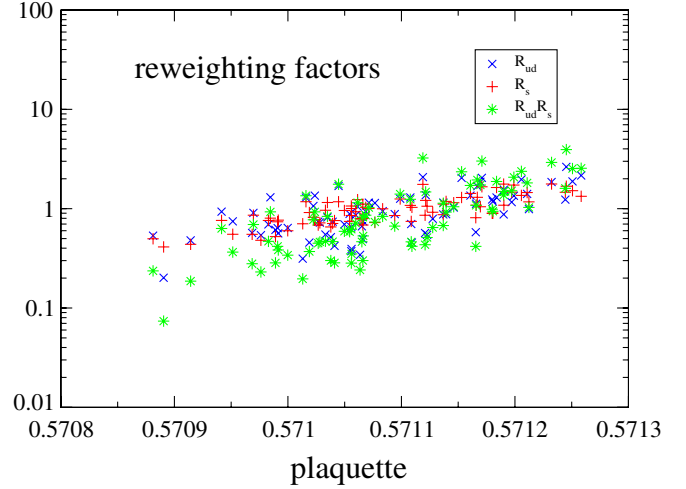
such that the distributions of observable fail to overlap each other. This problematic case could be detected by monitoring the behavior of the expectation value for the observable as the reweighting parameters are monotonically moved from the original point: The expectation value of the observable stops varying with diminishing error bar. To check the reliability of our reweighting procedure we have investigated the behavior of the expectation value of the plaquette against the reweighting with respect to the strange quark from $\kappa_{\text{s}} = 0.136\,600\,00$ to $\kappa_{\text{s}} = 0.136\,690\,00$ with $N_B = 4$ and 8, the latter of which yields the same amount of breakup interval as $\Delta_{\text{s}} = (0.136\,633\,75 - 0.136\,600\,00)/3 = 0.000\,011\,25$ in our choice. Since the plaquette value has much narrower distribution than the hadron propagators at each time slice, this is a stringent test to check the overlap of the distributions of the observable at the original and the target points.
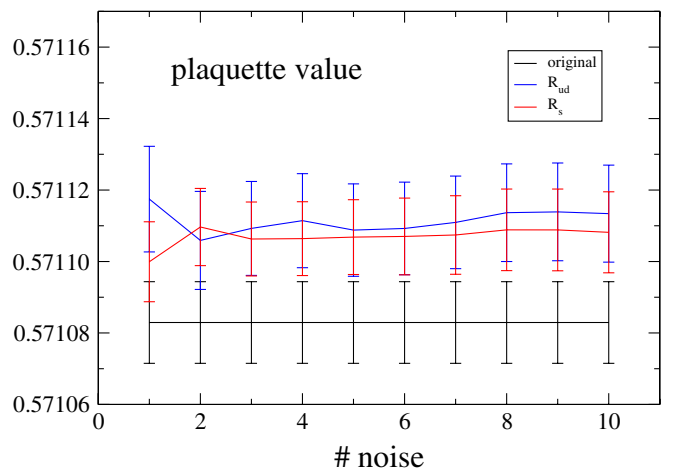

FIG. 3 (color online). Reweighted plaquette values with R_{ud} and R_{s} as a function of the number of noise.
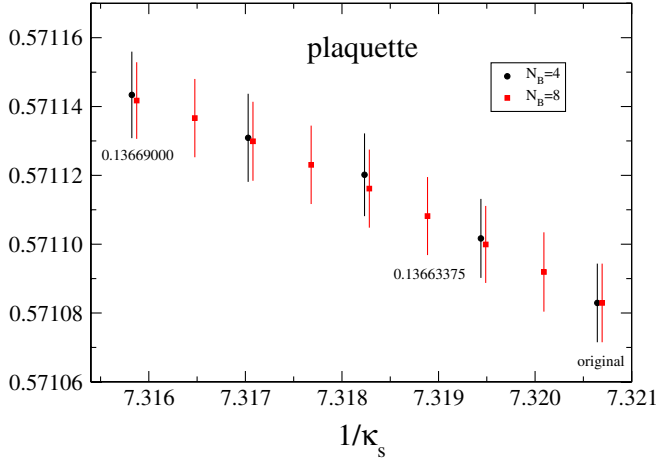
FIG. 4 (color online).   Reweighted plaquette values with R_s as a function of target value of κ_s. Interval from $\kappa_s = 0.136\,600\,00$ to $0.136\,690\,00$ is divided by $N_B = 4$ (black) and 8 (red).
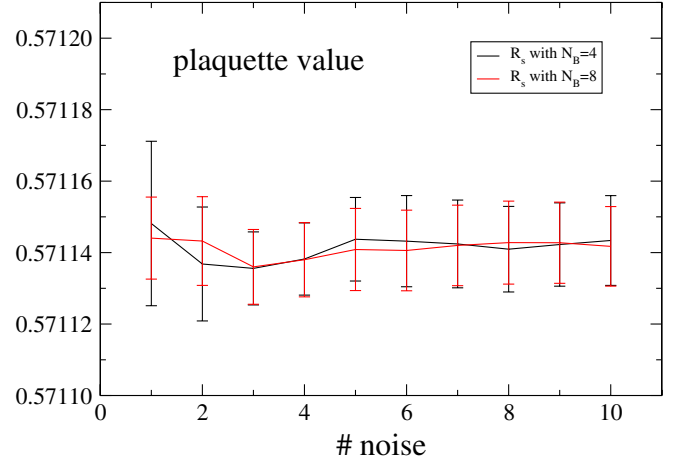

FIG. 6 (color online).   Reweighted plaquette value with R_s from $\kappa_s = 0.136\,600\,00$ to $0.136\,690\,00$ as a function of the number of noise. Interval is divided by $N_B = 4$ (black) and 8 (red).

Figure 4 shows the behavior of the reweighted plaquette value evaluated with 10 noise sources as a function of the reweighting parameter κ_s. We do not observe any sign that the reweighted plaquette value stagnates at some point: It shows almost linear behavior with constant magnitude of error up to $\kappa_s = 0.136\,690\,00$ which is far beyond the physical point of $\kappa_s = 0.136\,633\,75$. Furthermore $N_B = 4$ and 8 cases give consistent results. In Fig. 5 we plot the reweighting factor R_s from $\kappa_s = 0.136\,600\,00$ to $\kappa_s = 0.136\,690\,00$ with $N_B = 4$ and 8 as a function of the plaquette value on each configuration, which is normalized as $\langle R_s \rangle = 1$. Both cases show quite similar distributions, which confirm that our choice of breakup interval $\Delta_s = 0.000\,011\,25$ is sufficiently small. In Fig. 6 we also present the reweighted plaquette value with R_s as a function of the number of noise. The results with $N_B = 4$ and 8 become

FIG. 5 (color online).   Reweighting factor R_s from $\kappa_s = 0.136\,600\,00$ to $0.136\,690\,00$ with $N_B = 4$ (black) and 8 (red) as a function of plaquette value.

fairly consistent once we employ more than two noise sources. We have repeated the same analyses for the reweighting with respect to the ud-down quark from $\kappa_s = 0.137\,785\,00$ to $\kappa_s = 0.137\,800\,00$ with $N_B = 2$ and 4. The same conclusion is obtained as in the strange quark case. This is easily expected from similar behaviors for R_{ud} and R_s found in Figs. 1–3.

IV. HADRONIC OBSERVABLES

A. Hadron masses, quark masses and decay constants at simulation point

We measure the meson and the baryon correlators employing appropriate operators. The general form of the meson operators is expressed as

$$M_\Gamma^{fg}(x) = \bar{q}_f(x)\Gamma q_g(x), \tag{23}$$

where f and g denote quark flavors and Γ are 16 Dirac matrices $\Gamma = \mathrm{I}, \gamma_5, \gamma_\mu, i\gamma_\mu\gamma_5$ and $i[\gamma_\mu, \gamma_\nu]/2$ ($\mu, \nu = 1, 2, 3, 4$). The octet baryon operators are given by

$$\mathcal{O}_\alpha^{fgh}(x) = \epsilon^{abc}((q_f^a(x))^T C\gamma_5 q_g^b(x))q_{h\alpha}^c(x), \tag{24}$$

where a, b, c are color indices, $C = \gamma_4\gamma_2$ is the charge conjugation matrix and $\alpha = 1, 2$ labels the z-component of the spin 1/2. The Σ- and Λ-like octet baryons are distinguished by the flavor structures:

$$\Sigma\text{-like:} \quad -\frac{\mathcal{O}^{[fh]g} + \mathcal{O}^{[gh]f}}{\sqrt{2}}, \tag{25}$$

$$\Lambda\text{-like:} \quad \frac{\mathcal{O}^{[fh]g} - \mathcal{O}^{[gh]f} - 2\mathcal{O}^{[fg]h}}{\sqrt{6}}, \tag{26}$$

where $O^{[fg]h} = \mathcal{O}^{fgh} - \mathcal{O}^{gfh}$. We define the decuplet baryon operators for the four z-components of the spin
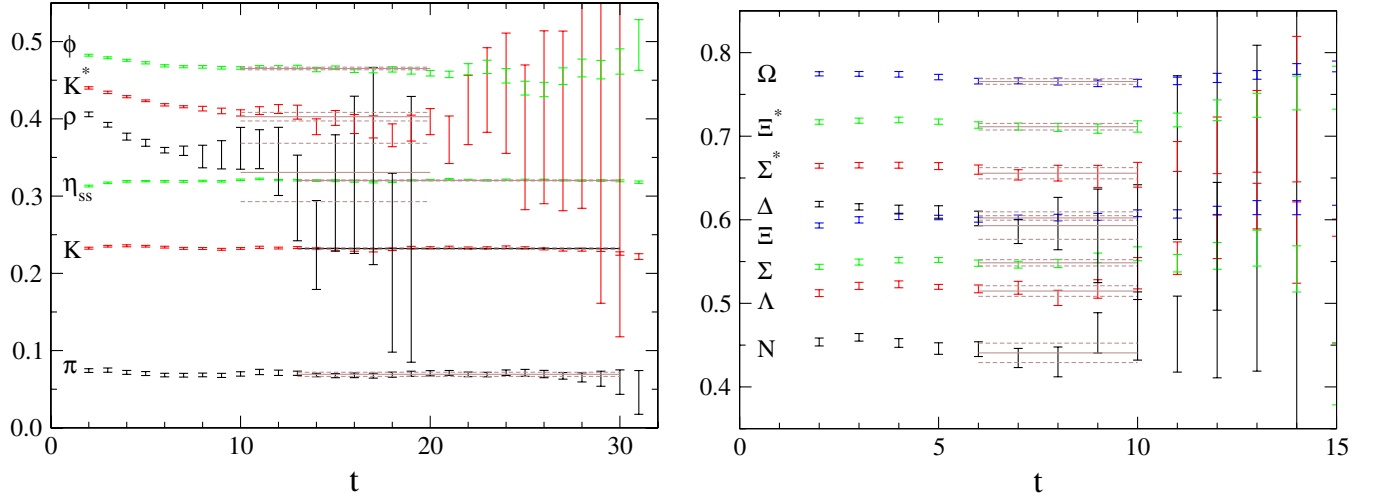
FIG. 7 (color online). Effective masses for the mesons (left) and the baryons (right) at the simulation point of $(\kappa_{ud}, \kappa_s) =$ (0.137 785 00, 0.136 600 00). Horizontal bars represent the fit results with 1 standard deviation error band.

3/2 as

$$D_{3/2}^{fgh}(x) = \epsilon^{abc}((q_f^a(x))^T C\Gamma_+ q_g^b(x))q_{h1}^c(x), \qquad (27)$$

$$D_{1/2}^{fgh}(x) = \epsilon^{abc}[((q_f^a(x))^T C\Gamma_0 q_g^b(x))q_{h1}^c(x)$$
$$- ((q_f^a(x))^T C\Gamma_+ q_g^b(x))q_{h2}^c(x)]/3, \qquad (28)$$

$$D_{-1/2}^{fgh}(x) = \epsilon^{abc}[((q_f^a(x))^T C\Gamma_0 q_g^b(x))q_{h2}^c(x)$$
$$- ((q_f^a(x))^T C\Gamma_- q_g^b(x))q_{h1}^c(x)]/3, \qquad (29)$$

$$D_{-3/2}^{fgh}(x) = \epsilon^{abc}((q_f^a(x))^T C\Gamma_- q_g^b(x))q_{h2}^c(x), \qquad (30)$$

where $\Gamma_\pm = (\gamma_1 \mp \gamma_2)/2$, $\Gamma_0 = \gamma_3$ and the flavor structures should be symmetrized.

The meson and the baryon correlators are calculated with point and smeared sources and a local sink. The smeared source is constructed with an exponential smearing function $\Psi(|\vec{x}|) = A_q \exp(-B_q|\vec{x}|)$ (q = ud, s) where $\Psi(0) = 1$ for the ud and s quark propagators. Employing a couple of thermalized configurations we adjust the parameters such that the pseudoscalar meson effective masses reach a plateau as soon as possible. Our choice is $A_{ud} = 1.2$, $B_{ud} = 0.07$ and $A_s = 1.2$, $B_s = 0.18$.

To reduce the statistical error of the zero momentum hadron correlators we employ two methods. One is the choice of four source points at $(x_0, y_0, z_0, t_0) = (17, 17, 17, 1)$, $(1, 1, 1, 9)$, $(25, 25, 25, 17)$, and $(9, 9, 9, 25)$. The other is the use of possible spin states: three polarization states for the vector meson and two (four) spin states for the octet (decuplet) baryons. The correlators with different sources and spin states are averaged on each configuration before the jackknife analysis.

Figure 7 shows effective mass plots for the meson and baryon propagators with the smeared source, where we

assume a single hyperbolic cosine function for the former and a single exponential form for the latter. We observe good plateaux starting at small values of t, showing that the excited state contributions are suppressed. The hadron masses are extracted by uncorrelated χ^2 fit to the propagators, since we find instabilities in correlated fit using covariance matrix. The horizontal bars in Fig. 7 represent the fit ranges, which are $[t_{min}, t_{max}] = [13, 30]$ for the pseudoscalar mesons, [10, 20] for the vector mesons and [6, 10] for the baryons, and the resulting hadron masses with 1 standard deviation error band. The numerical values are summarized in Table II. The statistical errors are estimated with the jackknife method. In Fig. 8 we plot the binsize dependence of the error for the pseudoscalar meson masses. The magnitude of error shows flat behaviors

TABLE II. Meson and baryon masses in lattice units at original and target points.

|	original	target	physical point in Ref. [9]
κ_{ud}	0.137 785 00	0.137 796 25	⋯
κ_s	0.136 600 00	0.136 633 75	⋯
π	0.0693(27)	0.0617(28)	0.0620(9)
K	0.2321(10)	0.2270(9)	0.2287(33)
η_{ss}	0.3203(7)	0.3138(6)	0.3168(43)
ρ	0.331(38)	0.272(39)	0.357(16)
K^*	0.4028(55)	0.393(11)	0.4118(72)
ϕ	0.4652(17)	0.4605(28)	0.4634(61)
N	0.441(12)	0.447(21)	0.438(20)
Λ	0.5147(63)	0.518(10)	0.502(10)
Σ	0.5485(38)	0.5484(62)	0.531(11)
Ξ	0.6022(27)	0.6001(28)	0.5991(75)
Δ	0.593(16)	0.587(27)	0.587(19)
Σ^*	0.6557(67)	0.658(12)	0.657(15)
Ξ^*	0.7114(39)	0.7113(53)	0.718(12)
Ω	0.7655(34)	0.7624(34)	0.769(11)
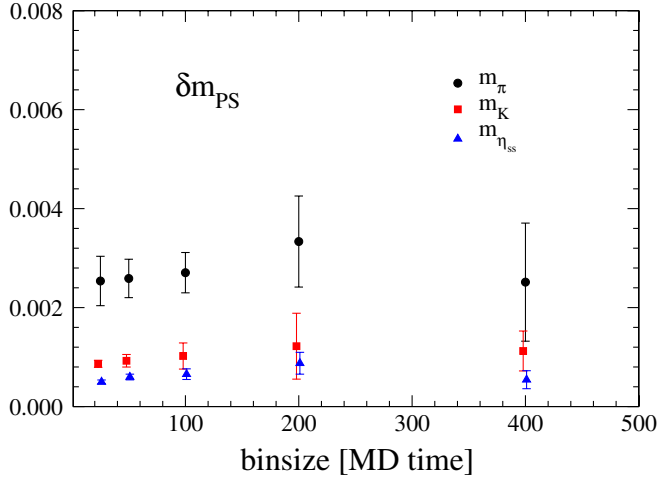
FIG. 8 (color online).   Bin size dependence of the magnitude of error for the pseudoscalar meson masses.

against the binsize within the error bars. Since similar bin size dependences are found for other particle types, we employ a binsize of 100 MD time (4 gauge configurations) for the jackknife analysis. As a cross check we also carry out the bootstrap error estimation with 5000 samples. For all the physical quantities at the original and the target points the bootstrap samples show clear normal distribution and the error estimates agree with those of the jack-knife method within 10%.

For the quark masses and the decay constants we have accomplished an important improvement since the previous publication [9]: a nonperturbative determination of renormalization factors based on the Schödinger functional scheme [25–27]. The bare quantities are calculated with the same method as in Ref. [9].

The bare quark mass is defined by the axial vector Ward-Takahashi identity (AWI):

$$\bar{m}_f^{\mathrm{AWI}} + \bar{m}_g^{\mathrm{AWI}} = \frac{\langle 0|\nabla_4 A_4^{\mathrm{imp}}|\mathrm{PS}\rangle}{\langle 0|P|\mathrm{PS}\rangle}, \qquad (31)$$

where P is the pseudoscalar operator and $|\mathrm{PS}\rangle$ denotes the pseudoscalar meson state at rest consisting of f and g (f, $g = \mathrm{ud}$, s) valence quarks. The axial vector current is nonperturbatively $O(a)$-improved as $A_4^{\mathrm{imp}} = A_4 + c_A \bar{\nabla}_4 P$ with $\bar{\nabla}_4$ the symmetric lattice derivative and $c_A = -0.038\,761\,06$ [28]. The ratio of the matrix elements is evaluated by

$$\bar{m}_f^{\mathrm{AWI}} + \bar{m}_g^{\mathrm{AWI}} = m_{\mathrm{PS}} \left| \frac{C_A^s}{C_P^s} \right|, \qquad (32)$$

where m_{PS}, C_A^s and C_P^s are extracted from a simultaneous χ^2 fit to

$$\langle A_4^{\mathrm{imp}}(t)P^s(0)\rangle = 2C_A^s \frac{\sinh(-m_{\mathrm{PS}}(t - T/2))}{\exp(m_{\mathrm{PS}}T/2)} \qquad (33)$$

and

$$\langle P(t)P^s(0)\rangle = 2C_P^s \frac{\cosh(-m_{\mathrm{PS}}(t - T/2))}{\exp(m_{\mathrm{PS}}T/2)} \qquad (34)$$

with P^s the smeared pseudoscalar operator and $T = 64$ the temporal extent of the lattice. The fit ranges are chosen to be $[t_{\min}, t_{\max}] = [13, 25]$ for the former and $[13, 30]$ for the latter. The renormalized quark mass in the continuum $\overline{\mathrm{MS}}$ scheme is defined as

$$m_f^{\overline{\mathrm{MS}}} = Z_m^{\overline{\mathrm{MS}}} \bar{m}_f^{\mathrm{AWI}}, \qquad (35)$$

where $Z_m^{\overline{\mathrm{MS}}} = Z_A/Z_P$ is nonperturbatively determined in the Schrödinger functional scheme. In Table IV we present the results for $m_{\mathrm{ud}}^{\overline{\mathrm{MS}}}$ and $m_s^{\overline{\mathrm{MS}}}$ renormalized at $\mu = 2$ GeV together with the corresponding bare quark masses $\bar{m}_f^{\mathrm{AWI}}$ and $\bar{m}_s^{\mathrm{AWI}}$. We use $Z_m^{\overline{\mathrm{MS}}}(2$ GeV$) = 1.441(15)$ [27]. The
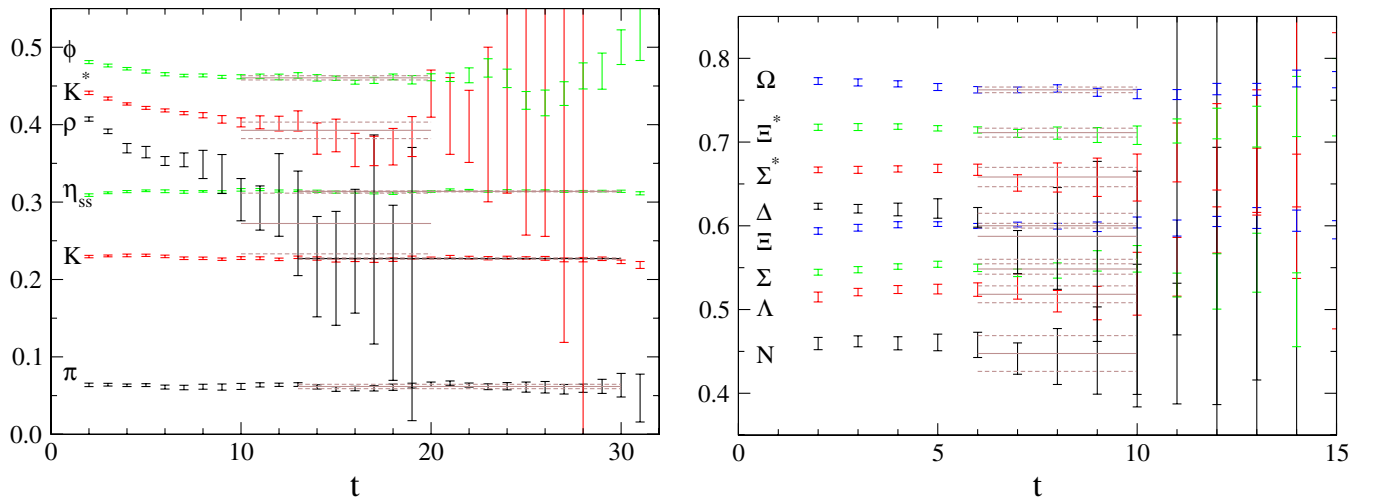

FIG. 9 (color online).   Effective masses for the mesons (left) and the baryons (right) at the target point of $(\kappa_{\mathrm{ud}}^*, \kappa_{\mathrm{s}}^*) = (0.137\,796\,25, 0.136\,633\,75)$. Horizontal bars represent the fit results with 1 standard deviation error band.

TABLE III. Meson and baryon masses in physical units at target point. Experimental value for $m_{\eta_{ss}}$ is estimated by $m_{\eta_{ss}} = \sqrt{2m_K^2 - m_\pi^2}$.

	target [GeV]	physical point in Ref. [9] [GeV]	experiment [GeV] [29]
κ_{ud}	0.137 796 25	$\cdots$	$\cdots$
κ_s	0.136 633 75	$\cdots$	$\cdots$
π	0.1354(62)	$\cdots$	0.1350
K	0.4980(22)	$\cdots$	0.4976
η_{ss}	0.6884(32)	0.6895(20)	0.6906
ρ	0.597(86)	0.776(34)	0.7755
K^*	0.861(23)	0.896(9)	0.8960
ϕ	1.0102(77)	1.0084(40)	1.0195
N	0.982(45)	0.953(41)	0.9396
Λ	1.137(25)	1.092(20)	1.1157
Σ	1.203(11)	1.156(17)	1.1926
Ξ	1.3165(60)	1.304(10)	1.3148
Δ	1.289(59)	1.275(39)	1.232
Σ^*	1.444(25)	1.430(23)	1.3837
Ξ^*	1.560(10)	1.562(9)	1.5318
Ω	$\cdots$	$\cdots$	1.6725

statistical errors are estimated by the jackknife analysis with the choice of the same bin size as for the hadron masses.

The bare pseudoscalar meson decay constant defined by

$$\sqrt{2\kappa_f}\sqrt{2\kappa_g}|\langle 0|A_4^{\text{imp}}|\text{PS}\rangle| = f_{\text{PS}}^{\text{bare}} m_{\text{PS}}. \quad (36)$$

is evaluated from the following formula:

$$f_{\text{PS}}^{\text{bare}} = \sqrt{2\kappa_f}\sqrt{2\kappa_g}\left|\frac{C_A^s}{C_P^s}\right|\sqrt{\frac{2|C_P^l|}{m_{\text{PS}}}}. \quad (37)$$

We extract m_{PS}, C_A^s, C_P^s, and C_P^l from a simultaneous fit of Eqs. (33) and (34) and

$$\langle P(t)P^l(0)\rangle = 2C_P^l \frac{\cosh(-m_{\text{PS}}(t - T/2))}{\exp(m_{\text{PS}}T/2)} \quad (38)$$

with P^l the local pseudoscalar operator. The fit ranges are [13, 25], [13, 30], and [15, 25], respectively. The renormalization is given by

$$f_{\text{PS}} = Z_A f_{\text{PS}}^{\text{bare}}, \quad (39)$$
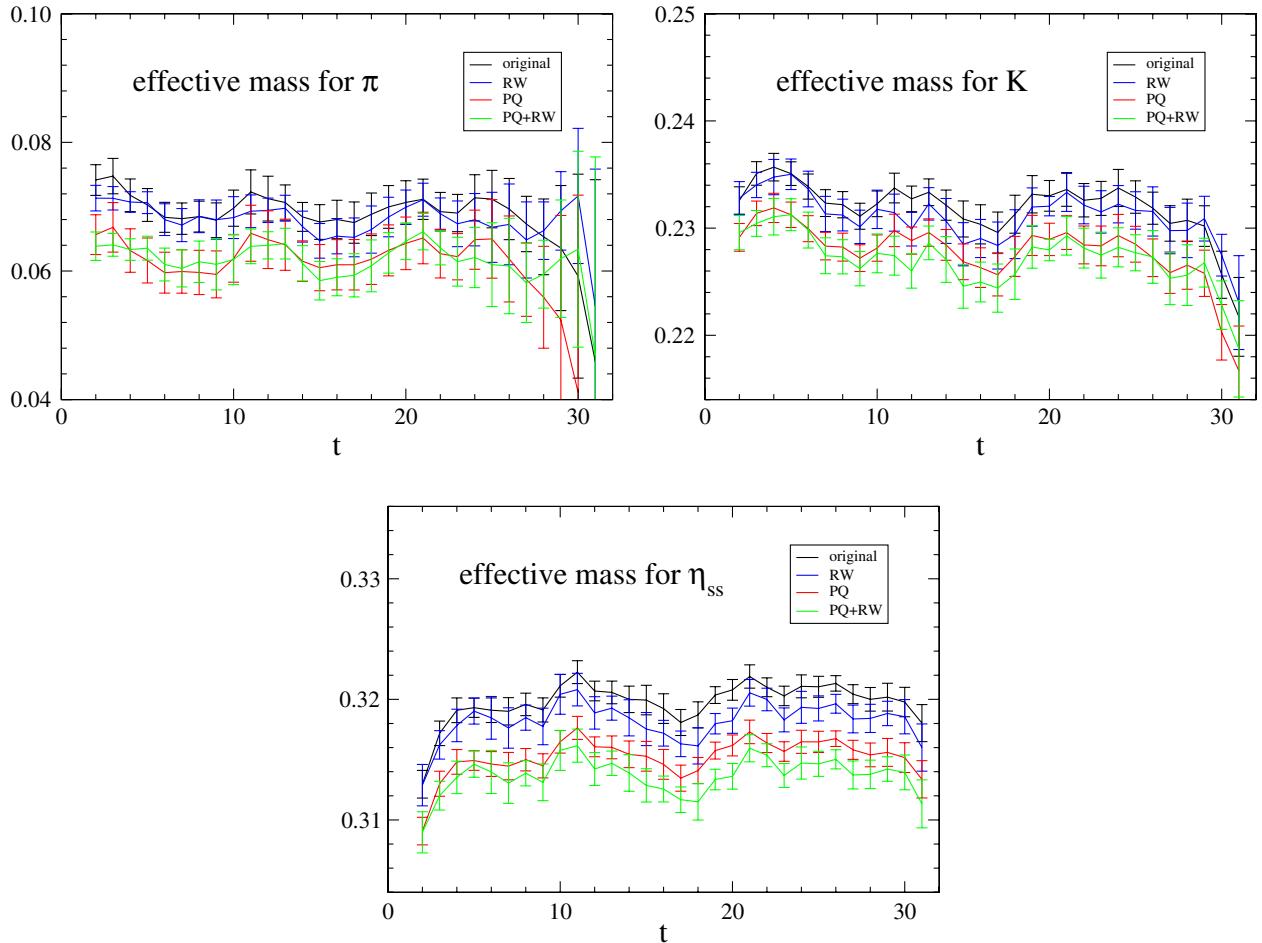
FIG. 10 (color online). π, K and η_{ss} effective masses with the reweighting factors from $(\kappa_{ud}, \kappa_s) = (0.137\,785\,00, 0.136\,600\,00)$ to $(\kappa_{ud}^*, \kappa_s^*) = (0.137\,796\,25, 0.136\,633\,75)$.

with $Z_A = 0.8563(52)$ [27] the nonperturbative renormal-
ization factor in the Schrödinger functional scheme. In
Table IV we list the results for f_{PS} and f_{PS}^{bare} with the
statistical errors evaluated in the same manner as for the
quark masses.

B. Hadron masses, quark masses and decay constants at target point

In Fig. 9 we present the effective masses for the re-
weighted meson and baryon propagators with the smeared
source. Comparing with the original case in Fig. 7 the error
bars are slightly enlarged by the reweighting procedure.
We apply the uncorrelated χ^2 fit to the reweighted hadron
propagators at the target point choosing the same fit ranges
and jackknife bin size as in the simulation point. The
results are summarized in Tables II and III, where we
also present the previous results obtained by the chiral
extrapolation method in Ref. [9] for comparison.

To investigate the reweighting effects on the hadron
effective masses, we show the effective masses for the
pseudoscalar mesons with and without the reweighting
factors in Fig. 10, where η_{ss} is a fictitious pseudoscalar
meson consisting of two strange quarks. For all the cases
the partially quenched results (PQ) show lighter effective
masses than the unitary results at the simulation point.
They are further reduced by the reweighting procedure
(PQ + RW). For other hadron channels the reweighting
effects are less clear partly because of the larger error bars.

In Fig. 11 we plot the π, ρ and nucleon masses at the
target point as a function of the number of noise. The
situation is quite similar to the plaquette case: Five or six
noises appear sufficient to obtain a reliable estimate. This
is also the case for other hadron masses.

Figure 12 compares the measured hadron masses nor-
malized by m_Ω with the experimental values. The results
for m_π/m_Ω and m_K/m_Ω, which are sizably deviated from
the experimental values at the simulation point (black
symbols), are properly tuned to the physical values
within error bars at the target point of $(\kappa_{ud}^*, \kappa_s^*) =$
$(0.137\,796\,25, 0.136\,633\,75)$. The lattice spacing is deter-
mined as $a = 0.08995(40)$ fm from m_Ω. A large discrep-
ancy found for m_ρ/m_Ω may be resolved by a proper
treatment of ρ meson as the resonance [30,31]. We plan
to do so for the ρ, K^* mesons and Δ baryon. For other
hadron masses we find less than 5% deviation from the
experimental values. An increasingly larger deviation ob-
served for lighter baryons may be due to finite size effects.

Possible finite size effects on the pseudoscalar meson
masses based on the NLO formulae of ChPT [32] are
discussed in Sec. IV D of Ref. [9]. The expected correc-
tions are less than 2% for m_π and m_K at the physical point.
The magnitude is smaller than the statistical errors found in
Table III. For the baryon masses the heavy baryon ChPT
predicts less than 1% corrections at the physical point on
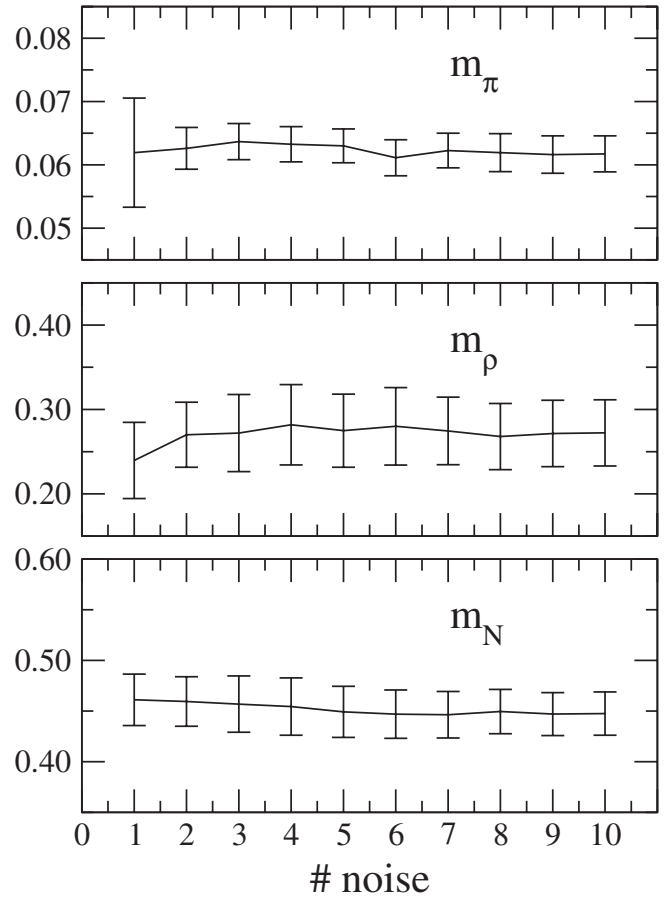our physical volume as listed in Table X of Ref. [10].

FIG. 11. π, ρ and nucleon masses as a function of the number of noise.

Although Fig. 12 clearly shows that further tuning is not
really necessary, it would be instructive to pin down the
physical point in the $(1/\kappa_{ud}, 1/\kappa_s)$ plane. The physical
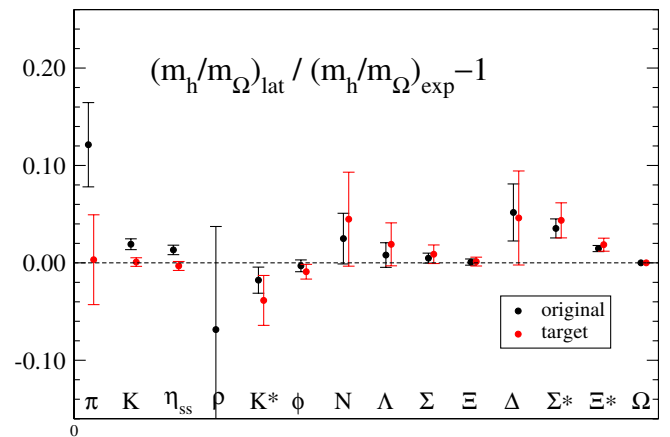point plotted in Fig. 13 is determined by a combined linear

FIG. 12 (color online).   Hadron masses normalized by m_Ω in
comparison with experimental values. Target result for ρ meson
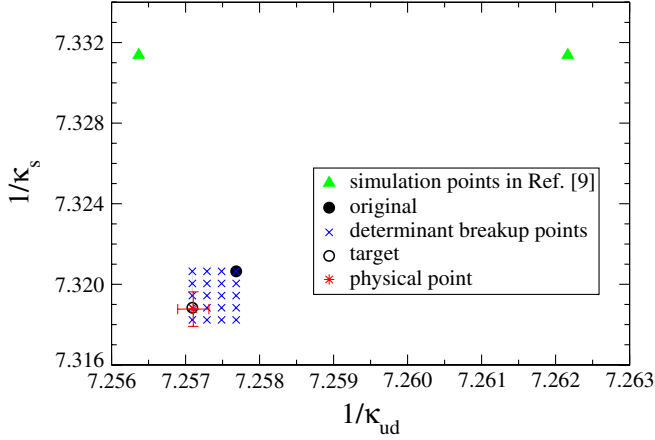locates below the figure.

FIG. 13 (color online). Determination of the physical point with m_π/m_Ω and m_K/m_Ω inputs in $(1/\kappa_{ud}, 1/\kappa_s)$ plane. Solid and open black circles denote the original and target points, respectively. Green symbols represent $(\kappa_{ud}, \kappa_s) =$ (0.137 810 00, 0.136 400 00) and (0.137 700 00, 0.136 400 00) which are lightest two simulation points in Ref. [9].

fit of $(m_\pi/m_\Omega)^2$ and $(m_K/m_\Omega)^2$ at $(\kappa_{ud}, \kappa_s) =$ (0.137 785 00, 0.136 600 00), $(\kappa_{ud}^*, \kappa_s^*) =$ (0.137 796 25, 0.136 633 75) and two more reweighted points given by (0.137 796 25, 0.136 633 75 $\pm \Delta_s$). The fit functions are

$$\left(\frac{m_\pi}{m_\Omega}\right)^2 = c_0^\pi + \frac{c_1^\pi}{\kappa_{ud}} + \frac{c_2^\pi}{\kappa_s}, \tag{40}$$

$$\left(\frac{m_K}{m_\Omega}\right)^2 = c_0^K + \frac{c_1^K}{\kappa_{ud}} + \frac{c_2^K}{\kappa_s} \tag{41}$$

with $c_{0,1,2}^{\pi,K}$ free parameters. The experimental values of m_π/m_Ω and m_K/m_Ω are reproduced at $(\kappa_{ud}, \kappa_s) =$ (0.137 797(4), 0.136 635(16)), whose central value is almost exactly hit by our target point $(\kappa_{ud}^*, \kappa_s^*) =$ (0.137 796 25, 0.136 633 75).

The quark masses and the pseudoscalar decay constants are extracted by repeating the same analyses as in the simulation point. The results are summarized in Table IV. The quark masses are determined as $m_{ud}^{\overline{MS}}(2 \text{ GeV}) =$ 2.97(28)(03) MeV and $m_s^{\overline{MS}}(2 \text{ GeV}) = 92.75(58) \times$ (95) MeV with $a^{-1} = 2.194(10)$ GeV, where the second error is due to the nonperturbative renormalization factor obtained by the Schrödinger functional method [27]. We find that our quark masses are comparable to recent estimates in the literature [33]. The discrepancy between the quark masses in this work and those in Ref. [9] is mainly due to the difference in the renormalization factors. The nonperturbative estimate gives about 30% larger value than the perturbative one [27]. For the pseudoscalar meson decay constants we obtain $f_\pi = 124.1(8.5)(0.8)$ MeV and $f_K = 165.5(3.4)(1.0)$ MeV with the second error coming from the nonperturbative renormalization factor [27]. These values should be compared with experiment: $f_\pi = 130.4 \pm 0.04 \pm 0.2$ MeV and $f_K = 155.5 \pm 0.2 \pm 0.8 \pm 0.2$ MeV [29]. Note that the NLO ChPT analyses predict 4% (1.5%) deficit for f_π (f_K) on a $(3 \text{ fm})^3$ box at the physical point due to the finite size effects [9,32].

V. CONCLUSION

We have presented the results of the physical point simulation in $2 + 1$ flavor lattice QCD with the $O(a)$-improved Wilson quark action. This is accomplished by two algorithmic ingredients: the DDHMC algorithm with several improvements and the reweighting technique. The former contributes to cost reduction and the latter is required for fine-tuning to the physical point.

Clear reweighting effects are observed on several observables: The plaquette value increases and the hadron masses are reduced in agreement with the expectation for the reweighting from the simulation point at $(\kappa_{ud}, \kappa_s) =$ (0.137 785 00, 0.136 600 00) to the target point at $(\kappa_{ud}^*, \kappa_s^*) = (0.137 796 25, 0.136 633 75)$. We are allowed to properly tune the measured values of m_π, m_K, and m_Ω to their experimental ones.

TABLE IV. Quark masses and pseudoscalar decay constants at original and target points. Renormalization factors are nonperturbative in this work, while perturbative in Ref. [9].

	original	target	physical point in Ref. [9]	experiment [29]
κ_{ud}	0.137 785 00	0.137 796 25	$\cdots$	$\cdots$
κ_s	0.136 600 00	0.136 633 75	$\cdots$	$\cdots$
$a\bar{m}_{ud}^{AWI}$	0.001 241(95)	0.000 939(87)	0.001 042(32)	$\cdots$
$a\bar{m}_s^{AWI}$	0.030 44(9)	0.029 34(12)	0.029 99(70)	$\cdots$
$m_{ud}^{\overline{MS}}$ [MeV]	3.92(30)(04)	2.97(28)(03)	2.527(47)	$\cdots$
$m_s^{\overline{MS}}$ [MeV]	96.23(52)(98)	92.75(58)(95)	72.72(78)	$\cdots$
m_s/m_{ud}	24.5(1.8)	31.2(2.7)	28.78(40)	$\cdots$
af_π^{bare}	0.0701(35)	0.0661(45)	0.0753(22)	$\cdots$
af_K^{bare}	0.0898(16)	0.0881(19)	0.0897(18)	$\cdots$
f_π [MeV]	131.7(6.6)(0.8)	124.1(8.5)(0.8)	134.0 (4.2)	$130.4 \pm 0.04 \pm 0.2$
f_K [MeV]	168.7(2.7)(1.0)	165.5(3.4)(1.0)	159.4 (3.1)	$155.5 \pm 0.2 \pm 0.8 \pm 0.2$
f_K/f_π	1.280(60)	1.333(72)	1.189(20)	$\cdots$

We extract the hadron masses, the quark masses and the pseudoscalar decay constants directly on the physical point after the reweighting procedure. For the hadron masses we find less than 5% deviation from the experimental values except the ρ meson case which requires a proper analysis as the resonance. The results for the quark masses renormalized in the $\overline{\text{MS}}$ scheme at $\mu = 2$ GeV are presented with the nonperturbative renormalization factor determined by the Schrödinger functional method. The large enhancement of the quark masses compared to those in Ref. [9] is attributed to the difference between the nonperturbative renormalization factor and the perturbative one.

The physical point simulation, which has been the long-standing problem in lattice QCD, is achieved in this work. It appears to us that it is not worthwhile to increase the statistics with the present simulation parameters. More important as the next step is to repeat the physical point simulation with larger and finer lattices. Further reduction of the finite size effects and the finite cutoff effects will make possible precision measurements of physical observables at 1% level.

[1] S. Aoki *et al.* (PACS-CS Collaboration), Proc. Sci. LAT2005 (2006) 111.

[2] A. Ukawa *et al.* (PACS-CS Collaboration), Proc. Sci. LAT2006 (2006) 039.

[3] T. Boku *et al.*, *Proceedings of CCGRID 2006* (2006), p. 233.

[4] S. Aoki *et al.* (CP-PACS and JLQCD Collaborations), Phys. Rev. D **73**, 034501 (2006).

[5] Y. Iwasaki, Report No. UTHEP-118, 1983 (unpublished).

[6] M. Lüscher, J. High Energy Phys. 05 (2003) 052; Comput. Phys. Commun. **165**, 199 (2005).

[7] M. Hasenbusch, Phys. Lett. B **519**, 177 (2001).

[8] M. Hasenbusch and K. Jansen, Nucl. Phys. **B659**, 299 (2003).

[9] S. Aoki *et al.* (PACS-CS Collaboration), Phys. Rev. D **79**, 034503 (2009).

[10] K.-I. Ishikawa *et al.* (PACS-CS Collaboration), Phys. Rev. D **80**, 054502 (2009).

[11] A. M. Ferrenberg and R. H. Swendsen, Phys. Rev. Lett. **61**, 2635 (1988).

[12] T. Ishikawa *et al.* (CP-PACS and JLQCD Collaborations), Phys. Rev. D **78**, 011502 (2008).

[13] J. C. Sexton and D. H. Weingarten, Nucl. Phys. **B380**, 665 (1992).

[14] A. Kennedy, Nucl. Phys. B, Proc. Suppl. **140**, 190 (2005).

[15] R. Brower, T. Ivanenko, A. Levi, and K. Orginos, Nucl. Phys. **B484**, 353 (1997).

[16] M. Parks *et al.*, SIAM J. Sci. Comput. **28**, 1651 (2006).

[17] Ph. de Forcrand and T. Takaishi, Nucl. Phys. B, Proc. Suppl. **53**, 968 (1997).

[18] R. Frezzotti and K. Jansen, Phys. Lett. B **402**, 328 (1997); Nucl. Phys. **B555**, 395 (1999); **B555**, 432 (1999).

[19] S. Aoki *et al.* (JLQCD Collaboration), Phys. Rev. D **65**, 094507 (2002).

[20] K.-I. Ishikawa *et al.* (PACS-CS Collaboration), Proc. Sci. LAT2006 (2006) 027.

[21] C. Alexandrou, P. de Forcrand, M. D'Elia, and H. Panagopoulos, Phys. Rev. D **61**, 074503 (2000); Nucl. Phys. B, Proc. Suppl. **83**, 765 (2000); P. de Forcrand, Nucl. Phys. B, Proc. Suppl. **73**, 822 (1999).

[22] A. Boriçi and P. de Forcrand, Nucl. Phys. **B454**, 645 (1995); A. Borrelli, P. de Forcrand, and A. Galli, Nucl. Phys. **B477**, 809 (1996); P. de Forcrand and A. Galli, arXiv:hep-lat/9603011; A. Galli and P. de Forcrand, Nucl. Phys. B, Proc. Suppl. **53**, 956 (1997).

[23] A. Hasenfratz, R. Hoffmann, and S. Schaefer, Phys. Rev. D **78**, 014515 (2008).

[24] C. Jung, Proc. Sci. LAT2009 (2009) 002.

[25] S. Aoki *et al.* (PACS-CS Collaboration), J. High Energy Phys. 10 (2009) 053.

[26] Y. Taniguchi *et al.* (PACS-CS Collaboration), Proc. Sci. LAT2009 (2009) 208.

[27] S. Aoki *et al.* (PACS-CS Collaboration) (unpublished).

[28] T. Kaneko *et al.* (CP-PACS/JLQCD and ALPHA Collaborations), J. High Energy Phys. 04 (2007) 092.

[29] C. Amsler *et al.* (Particle Data Group), Phys. Lett. B **667**, 1 (2008).

[30] M. Lüscher, Commun. Math. Phys. **105**, 153 (1986); Nucl. Phys. **B354**, 531 (1991); **B364**, 237 (1991).

[31] S. Aoki *et al.* (CP-PACS Collaboration), Phys. Rev. D **76**, 094506 (2007).

[32] G. Colangelo, S. Dürr, and C. Haefeli, Nucl. Phys. **B721**, 136 (2005).

[33] For a recent review, see, E. Scholz, Proc. Sci. LAT2009 (2009) 005.